Brazilian Journal
of Chemical
Engineering

ISSN 0104-6632
Printed in Brazil
www.abeq.org.br/bjche

Vol. 26, No. 03, pp. 457 - 468, July - September, 2009

EXPERIMENTAL AND THEORETICAL INVESTIGATION OF ANAEROBIC FLUIDIZED BED BIOFILM REACTORS

M. Fuentes[1*], M. C. Mussati[1,2], P. A. Aguirre[1,3] and N. J. Scenna[1,2]

[1]INGAR, Instituto de Desarrollo y Diseño, Phone.: + (54) 342-4534451,
Fax: + (54) 342-4553439, Avellaneda 3657 (3000) Santa Fe, Argentina.
E-mail: mfuentes@santafe-conicet.gov.ar
[2]Departamento de Ingeniería Química, GIAIQ, UTN FRR, Zeballos 1341, (2000), Rosario, Argentina.
[3]Facultad de Ingeniería Química, UNL, Santiago del Estero 2829, (3000) Santa Fe, Argentina.

(Submitted: March 20, 2006 ; Revised: January 12, 2007 ; Accepted: January 29, 2007)

Abstract - This work presents an experimental and theoretical investigation of anaerobic fluidized bed reactors (AFBRs). The bioreactors are modeled as dynamic three-phase systems. Biochemical transformations are assumed to occur only in the fluidized bed zone. The biofilm process model is coupled to the system hydrodynamic model through the biofilm detachment rate; which is assumed to be a first-order function of the energy dissipation parameter and a second order function of biofilm thickness. Non-active biomass is considered to be particulate material subject to hydrolysis. The model includes the anaerobic conversion for complex substrate degradation and kinetic parameters selected from the literature. The experimental set-up consisted of two mesophilic (36±1ºC) lab-scale AFBRs (R1 and R2) loaded with sand as inert support for biofilm development. The reactor start-up policy was based on gradual increments in the organic loading rate (OLR), over a four month period. Step-type disturbances were applied on the inlet (glucose and acetic acid) substrate concentration (chemical oxygen demand (COD) from 0.85 to 2.66 g L^{-1}) and on the feed flow rate (from 3.2 up to 6.0 L d^{-1}) considering the maximum efficiency as the reactor loading rate switching. The predicted and measured responses of the total and soluble COD, volatile fatty acid (VFA) concentrations, biogas production rate and pH were investigated. Regarding hydrodynamic and fluidization aspects, variations of the bed expansion due to disturbances in the inlet flow rate and the biofilm growth were measured. As rate coefficients for the biofilm detachment model, empirical values of $3.73 \cdot 10^4$ and $0.75 \cdot 10^4$ s^2 kg^{-1} m^{-1} for R1 and R2, respectively, were estimated.
Keywords: Anaerobic Processes; Biofilms; Dynamic Modeling; Fluidized Bed Bioreactors; Wastewater Treatment.

INTRODUCTION

The successful design and operation of a biological fluidized bed reactor depend on the ability to accurately predict the fundamental characteristics of the system, specifically, the hydrodynamics, the mixing of individual phases, and the mass transfer properties (Muroyama and Fan, 1985). Fluidization characteristics such as fluidized bed height and phase holdups (volume fractions) are critical because of their influence on the residence time, specific biofilm superficial area in the biologically active zone, reactor size, mass transfer and biofilm detachment rate (Bonnet et al., 1997). Authors (Abdul-Aziz and Asolekar, 2000; Bonnet et al., 1997 ; Diez Blanco et al., 1995; Huang and Wu, 1996; Huang et al., 2000) have studied some aspects of the AFBR hydrodynamics hypothesizing a two-phase solid-liquid system because of the minimal amount of gas present, or as a three-phase gas-solid-liquid system (Yu and Rittmann, 1997) using the generalized wake and bubble model (GWBM) developed by Bathia and Epstein (1974) for describing the hydrodynamics. Many of these works consider

*To whom correspondence should be addressed

hydrodynamic steady state reactors and hypothetical steady state values of biofilm thickness. In this paper, the GWBM is also used, but a key feature of the model is the combination of the dynamic mass balance of the process components with the dynamic effects of the biofilm growth on the hydrodynamic characteristics such as holdups and the bed height during a biological transient. The aim of this work is to study the anaerobic treatment of a synthetic substrate using a fluidized bed reactor containing microorganisms inmobilized on sand particles and adjust an AFBR model from laboratory scale experimental data with emphasis on the evaluation of substrate utilization and gas production rates and pH evolution under different organic loading conditions at mesophilic temperature.

MATHEMATICAL MODEL

A dynamic model is proposed for representing variation of the properties such as phase holdups, biofilm thickness and biological and chemical species concentrations in a three phase (gas, solid, liquid) anaerobic reactor. The three phases present in the reactor are: (a) the solid phase consisting of the bioparticles composed of inert support material plus active and non-active attached biomass (biofilm); (b) the liquid phase containing substrates, products, enzymes, ions and active and non-active suspended biomass; and (c) the gas phase, which is a mixture of the gaseous fermentation products. Biochemical transformations are assumed to occur only in the fluidized bed zone. No mass transfer limitations in the biofilm and liquid film are assumed.

Anaerobic Digestion Model

The anaerobic digestion model proposed by Angelidaki et al. (1999) is assumed here. Figure 1 represents the digestion steps starting from biopolymers: carbohydrates, lipids and proteins. In this work, only carbohydrates and proteins are assumed as characteristic compounds of organic contamination. Because of this simplification, acidogenesis from glycerol combined with lipid (triglyceride) hydrolysis and acetogenesis from long chain fatty acids (LCFAs), numbered as steps (1) and (4) in Fig. 1, respectively, have not been modeled.

Carbohydrates and proteins are enzymatically hydrolyzed to soluble substrates, which are considered to be glucose and amino acids, respectively. As shown in Fig. 1, acidogen degraders use glucose and amino acids to produce a mixture of acetic, propionic, butyric and valeric acid. Then, valeric, butyric and propionic acetogens respectively convert valeric, butyric and propionic acids into acetic acid. As the specific growth rate of the hydrogen-utilizing methanogens is much faster than acetoclastic methanogens (degradation of acetic acid into methane and carbon dioxide), the hydrogen-utilizing methanogenic stage is combined with acetogenic stages (Angelidaki et al., 1993, 1999). Thus, the acetoclastic methanogens are only included in the model. The three components considered in the gas phase are methane, carbon dioxide and water vapor.

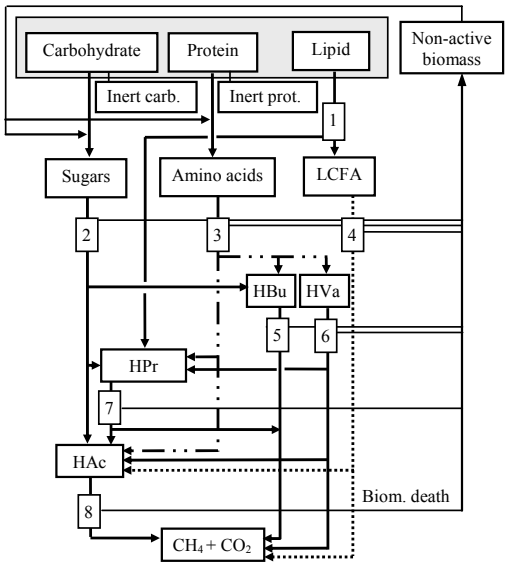

1. acidogenesis from glycerol combined with lipid (triglyceride) hydrolysis;
2. acidogenesis from sugars (glucose);
3. acidogenesis from amino acids;
4. acetogenesis from LCFA;
5. acetogenesis from butyrate (HBu);
6. acetogenesis from valerate (HVa);
7. acetogenesis from propionate (HPr);
8. acetoclastic methanogenesis.

Figure 1: Anaerobic digestion steps (Angelidaki et al., 1999)

Mass Balance Equations for Biological and Chemical Species

The sum of phase volume fractions (holdups) ε_k, k being either the liquid (k=L), the solid (k=S) or the gas phase (k=G), in the control volume defined by the expanded bed is equal to unity. For species of concentration φ_{ik}, the mass balance equations in the k-phases are, respectively:

$$d\frac{\varepsilon_L \varphi_{iL} V}{dt} = Q_{Lin}\varphi_{iL}^{*} - Q_{Lout}\varphi_{iL} + V\sum_j R_{iL}^j \quad (1)$$

$$d\frac{\varepsilon_S \varphi_{iS} V}{dt} = V\sum_j R_{iS}^j \quad (2)$$

$$d\frac{\varepsilon_G (v_{st} p_T \varphi_{iG}) V}{dt} = d\frac{\varepsilon_G p_i V}{dt} = -p_i Q_{Gout} + v_{st} p_T V\sum_j R_{iG}^j \quad (3)$$

where V is the volume of the fluidized bed, Q_{Lin} and Q_{Lout} are the liquid volumetric flows at the (expanded bed) reactor inlet and outlet, respectively, and φ_{iL}^{*} is the (mass or molar) concentration of the species i in the liquid phase at the reactor inlet. $\sum_j R_{ik}^j$ is the sum of all homogeneous and heterogeneous reaction and mass transfer and transport process rates where φ_{ik} (k=S,L,G) is involved. Q_{Gout} is the generated gas volumetric flow and p_i is the gas partial pressure. Table 1 includes the $\sum_j R_{ik}^j$ terms for the mass balances of active and non-active biological species (acidogens, acetogens and methanogens) in the solid and liquid phases, and the mass balances of soluble substrates and gas components.

X_i is the mass concentration of biological species i, suspended in the liquid fase (^{L}) or attached in the solid phase (^{S}), in active (act) or non-active (n-act) biological state. μ, b, k_E and K_{BH} are the specific rates of microorganism growth and death, biofilm detachment and hydrolysis of biomass, respectively. S_i denotes molar concentration of the soluble substrate for species i. $\lambda_{S_i}^j$ =-1, +1 or 0 depending on whether S_i is a substrate, an intermediate product or does not participate in the degradation stage j, respectively. Y_{S_i} is the yield coefficient characteristic of the substrate and is related to the degradation stage j. The specific growth and death rates of microorganisms are assumed to be the same for suspended and attached biomass of species i. In addition, the specific biomass hydrolysis rate is the same for all species. S_{ins_i} is the concentration of the insoluble substrate (carbohydrates and proteins) subject to hydrolysis. K_{Hid} is the specific hydrolysis rate. There is a relationship between K_{BH} and K_{Hid} since non-active biomass is considered as particulate material subject to hydrolysis (Angelidaki et al., 1999). The detachment rate is modeled as a first-order function of the specific energy dissipation rate ω in the gas-solid-liquid fluidized bed zone ($\omega = U_o(\Delta p/\Delta z)$; Huang and Wu, 1996), as a second-order function of the biofilm thickness δ and a first-order function of the mass concentration of each species i (see the term $k_E\omega\delta^2 X_i^S$, Table 1). k_E is assumed to be the same for all biological species and must be estimated from experimental data (Mussati et al., 2005a).

Methane is considered to be insoluble in the liquid phase; consequently, methane production rate equals the liquid-gas mass transfer rate ($\sum_j \lambda_{S_i}^j \frac{\mu_j}{Y_{S_i}^j}\left(\varepsilon_S X_{j_{act}}^S + \varepsilon_L X_{j_{act}}^L\right) - \varepsilon_L K_{Ti}(S_i - K_{Hi}p_i) = 0$, Table 1). K_{Hi} and K_{Ti} represent the Henry´s coefficient and total liquid-gas mass transfer coefficient, respectively. v_{st} is the gas molar volume. Antoine´s equation for calculating $p_{H_2O_{vapor}}$ is used.

Kinetics and Equilibrium in Solution Models

The kinetic model expressions of the specific microorganism growth rate (μ) and the equilibrium in solution model for calculating pH have been previously published (Angelidaki et al. 1999; Mussati et al., 2005a). The equilibrium in solution model includes mass balance equations for carbonate (inorganic carbon), ammonium-ammonia, phosphate, other anions and other cations and monoprotic acids (acetic, propionic, butyric and valeric acids) from degradation stages, and are involved in the system charge balance (electroneutrality condition) for calculating pH. Phosphate, other anions and other cations do not participate in the biochemical reactions ($\sum_j R_{ik}^j = 0$).

Table 1: $\sum_j R_{ik}^j$ terms of the species mass balance equations.

φ_{ik}	$\sum_j R_{ik}^j$	[1]Species i
$X_{i_{act}}^S$	$\varepsilon_S\left[\mu_i X_{i_{act}}^S - b_i X_{i_{act}}^S - k_E\omega\delta^2 X_{i_{act}}^S\right]$	Ac,Va,Bu,Pr,Aa,Gl
$X_{i_{n-act}}^S$	$\varepsilon_S\left[b_i X_{i_{act}}^S - K_{BH} X_{i_{n-act}}^S - k_E\omega\delta^2 X_{i_{n-act}}^S\right]$	Ac,Va,Bu,Pr,Aa,Gl
$X_{i_{act}}^L$	$\varepsilon_L\left[\mu_i X_{i_{act}}^L - b_i X_{i_{act}}^L\right] + \varepsilon_S k_E\omega\delta^2 X_{i_{act}}^S$	Ac,Va,Bu,Pr,Aa,Gl
$X_{i_{n-act}}^L$	$\varepsilon_L\left[b_i X_{i_{act}}^L - K_{BH} X_{i_{n-act}}^L\right] + \varepsilon_S k_E\omega\delta^2 X_{i_{n-act}}^S$	Ac,Va,Bu,Pr,Aa,Gl
S_{ins_i}	$-\frac{K_{Hid_i}}{Y_{S_i}^H}\varepsilon_L S_{ins_i}$	Aa,Gl[2]
S_i	$\sum_j \lambda_{S_i}^j \frac{\mu_j}{Y_{S_i}^j}\left(\varepsilon_S X_{j_{act}}^S + \varepsilon_L X_{j_{act}}^L\right) + \frac{K_{Hid_i}}{Y_{S_i}^H}\varepsilon_L S_{ins_i}$	Aa,Gl
S_i	$\sum_j \lambda_{S_i}^j \frac{\mu_j}{Y_{S_i}^j}\left(\varepsilon_S X_{j_{act}}^S + \varepsilon_L X_{j_{act}}^L\right)$	Ac,Va,Bu,Pr, IN,
S_i	$\sum_j \lambda_{S_i}^j \frac{\mu_j}{Y_{S_i}^j}\left(\varepsilon_S X_{j_{act}}^S + \varepsilon_L X_{j_{act}}^L\right) - \varepsilon_L K_{Ti}\left(S_i - K_{Hi} p_i\right)$	CH_4, IC (CO_2)
p_i	$\nu_{st} p_T \varepsilon_L K_{Ti}\left(S_i - K_{Hi} p_i\right)$	CH_4, CO_2

1. Referred to: acetate (Ac), valerate (Va), butyrate (Bu), propionate (Pr), amino acids (Aa), glucose (Gl), inorganic nitrogen (IN), inorganic carbon (IC), methane (CH_4) and carbon dioxide (CO_2).
2. S_{insAa} and S_{insGl} represent the protein and carbohydrate concentrations, respectively.

Bioparticle Model and Fluidization Characteristics

Homogeneous biofilm distribution on the support particles, constant density ρ_p and diameter d_p of the support particles, constant wet biofilm density and spherical geometry are assumed for the bioparticle model (Abdul-Aziz and Asolekar, 2000).

In bioreactors, the solid holdup varies during the biological transient due to the ongoing microbiological processes: growth, death, detachment and hydrolysis of biomass. An increase in the biofilm thickness δ causes an increase in the total height H of the fluidized bed, which is calculated as follows:

$$H = \frac{W}{\rho_p A \varepsilon_S}\left(1 + \frac{2\delta}{d_p}\right)^3 \tag{4}$$

where W and A are the initial particle load and column cross section area, respectively. Although microbiological processes cause changes in the hydrodynamic characteristics, the superficial velocity of the solid phase is practically zero compared to the liquid ones when the fluidized bed reactor reaches the hydrodynamic pseudo-steady state.

The simplified wake and bubble theory (i.e., the liquid wakes are particle-free) (Efremov and Vakhrushev, 1970; Yu and Rittmann, 1997) is used here to calculate the liquid holdup in a three phase fluidized bed system:

$$\varepsilon_L = \left(\frac{U_l}{U_t} - k\frac{U_g}{U_t}\right)^{1/n}\left(1 - \varepsilon_G - k\varepsilon_G\right)^{1-1/n} + k\varepsilon_G \tag{5}$$

In Eq. (5), U_l and U_g are the superficial liquid and gas velocities, respectively. k is the mean volume ratio of wake to bubbles which is calculated as (Yu and Rittmann, 1997):

$$k = 3.5\varepsilon_L^3 \exp\left(-5.08\varepsilon_G\right) \tag{6}$$

U_t is the terminal settling velocity of the particles and n is the bed expansion coefficient (Richardson and Zaki, 1954). In fluidized bed bioreactors, U_t and n are biofilm thickness functions. Authors (Hermanowicz and Ganzarczyk, 1983; Mulcahy and Shieh, 1987; Ngian and Marti, 1980; Setiadi, 1995; Thomas and Yates, 1985; Yu and Rittmann, 1997) have studied the effects of biofilm accumulation on these parameters in fluidized bed reactors. However, better concordance between experimental and predicted hydrodynamic values was obtained using the correlation formulated by Foscolo et al. (1983), even though it was not deduced to describe the hydrodynamics of AFBRs (Abdul-Aziz and Asolekar, 2000).

Here, the equation proposed by Foscolo et al. (1983) for calculating U_t is combined with the original equation proposed by Richardson and Zaki (1954) for calculating n:

$$U_t = \frac{-17.3\mu_L + \left[299.29\mu_L^{\,2} + 1.344 g d_{bp}^{\,3} \rho_L (\rho_S - \rho_L)\right]^{0.5}}{0.672 d_{bp} \rho_L}, \quad (7)$$

$$0.2 < Re_t < 500$$

$$n = 4.4\, Re_t^{-0.1}, 1 < Re_t < 500 \quad (8)$$

$$Re_t = \frac{U_t d_{bp} \rho_L}{\mu_L} \quad (9)$$

The empirical equation (Chern et al., 1984; Miyahara and Fan, 1992; Yu and Rittmann, 1997) for calculating ε_G directly from flow velocities and the solid holdup is used:

$$\frac{U_g}{\varepsilon_G} = \frac{U_g}{1-\varepsilon_S} + \frac{U_l}{1-\varepsilon_S} + 0.1016 + 1.488\left(\frac{U_l}{1-\varepsilon_S}\right)^{0.5} \quad (10)$$

A constant volumetric flow through the fluidized bed is assumed, the velocity in the bed cross section is equal to fluid velocity at the reactor inlet U_o.

Initial Conditions and Computational Aspects

Since the biofilm adsorption phenomenon is not modeled, low steady state concentration values are assigned as initial condition values for the biological and chemical species. The mathematical model was implemented and solved using the process modeling software tool gPROMS (Process Systems Enterprise Ltd). An additional programming effort was needed since a "high-index" differential algebraic equation (DAE) system (index>1) was verified. In high-index DAEs, the number of initial conditions that can be specified arbitrarily is less than the number of differential variables, the differential variables are not independent and ODE-type numerical methods fail. In this work, this problem was solved by rewriting the hydrodynamic variables as functions of biological species concentrations in order to provide the DAE system with a consistent initialization. The total CPU time for model simulations is about 33 seconds on an 800 MHz Pentium IV PC.

MATERIALS AND METHODS

Reactors and Supports

Two lab-scale anaerobic fluidized bed reactors (R1 and R2) were used to carry out the experiments. Both R1 and R2 consisted of acrylic columns with inside diameter of 0.065 m and height of 2.0 m. The separation compartment placed over the column is a 0.180 m high cylinder with a 0.145 m inner diameter, where gas accumulation and particle sedimentation take place. The effluent discharge, the feed input and the recycle suction point are also placed in this compartment. The operating temperature of the reactors was maintained at 36 ±1°C. The setup used for bioreactors was schematized in Mussati et al. (2005b, 2006). Bioreactor specifications are included in Table 2.

A sample of sand used in bioreactors R1 and R2 was meshed using the Tyler sieve series. The material specific surface and the surface volume mean diameter are calculated as in McCabe et al. (1993) and Perry and Chilton (1973). These values and other inert support characteristics have been included in Table 2.

The differences in the operational conditions of R1 and R2 are mainly based on the sand particle diameter used as inert support material. As shown in Table 2, bioreactor R2, which contains support particles with larger size than R1, operates at a higher superficial velocity of fluid than R1 to obtain similar fluidization characteristics (porosity varies from $\varepsilon_o \approx 0.4$ to $\varepsilon \approx 0.6$).

Table 2: Specification data for bioreactors R1 and R2 and support materials.

Specification	R1	R2
Bioreactor:		
Total sand-free volume (L)	8.40	8.10
Static bed porosity (L L^{-1})	0.42	0.40
Static bed volume (L)	2.32	2.49
Initial expanded bed volume (L)	3.50	3.58
Superficial velocity of fluid (U_o, $\times 10^2$ m s^{-1})	1.91	4.68
Inert support:		
Weight of dry sand loaded (kg)	3.50	4.00
Sand density (kg L^{-1})	2.63	2.66
Surface-vol. mean diameter (mm)	0.35	0.90
Specific surface (m^2 kg^{-1})	7.62	2.96

Table 3: Start-up policy of bioreactors R1 and R2.

Disturbance	Q_f (Ld^{-1})	OLR (g COD L^{-1} d^{-1})	TCOD (g COD L^{-1})	Time (d)
R1				
I	3.2	0.76	0.85	22
II	3.2	1.56	1.75	31
III	3.2	2.03	2.66	24
IV	4.3	2.73	2.66	17
V	6.0	3.80	2.66	16
R2				
I	3.2	0.76	0.85	19
II	3.2	1.56	1.75	31
III	3.2	2.37	2.66	24
IV	4.3	3.18	2.66	17
V	6.0	4.44	2.66	16

Analytical Methods

The amount of biogas produced by the bioreactor was measured using a water replacement method after gas washing using a $FeCl_3$ solution (pH 2) for removing H_2S. The gas composition was analyzed by a gas chromatograph (Hewlett Packard 6890) equipped with a thermal conductivity detector and a 3 m carbosphere column. Hydrogen was used as carrier gas at 20 mL min^{-1}. The column was operated at 150°C. The injector and detector temperatures were 100 and 230°C, respectively.

The effluent chemical oxygen demand (COD) was measured according to the HACH potassium dichromate method approved by USEPA (Cat. 21259-15, 0-1500 ppm). The concentration of the released Cr^{3+} ions was determined by spectrophotometry (Metrolab 330). Microfilters of PTFE 0.2 μm (F2513-4) were used for soluble COD (SCOD) determination. The effluent pH was measured using a digital pHmeter (Horiba D-12). The acetic, propionic and butyric acid (VFA) concentrations were measured by a high pressure liquid chromatograph (HPLC) Hewlett Packard Model Series 1050 equipped with a UV-VIS detector (wavelength: 215 nm). A 20 μL sample volume was injected into a Spherisorb ODS-1 (C18) Classic 5U (250 x 4.6 mm) column (Alltech, Deerfield, IL). The mobile phase consisted of 50% acetonitrile-50% water, sulfuric acid 0,01% (pH 3) at a flow rate of 0.7 mL min^{-1}.

Experimental Protocol

Fractions of both solid and liquid phases (500 mL, 9% volatile suspended solids) taken from an industrial upflow anaerobic sludge blanket (UASB) reactor treating a gelatin production wastewater were used as inoculums for reactors R1 and R2. The substrate consisted of a mixture of milk powder, acetate and glucose (10%, 20% and 70% of the total COD (TCOD), respectively) plus 0.1 g L^{-1} of NH_4Cl and 0.66 g L^{-1} of $NaHCO_3$, in order to provide the inoculums with the micro and macronutrients and adequate environmental conditions necessary for microbial growth. The start-up of the reactors involved stepped increases in COD loading and substrate concentration, over a four month period, following the time schedule presented in Table 3.

As shown in Table 3, the organic loading rate (OLR) was gradually increased from 0.76 to 2.03 g COD L^{-1} d^{-1} for R1, and 0.76 to 2.37 g COD L^{-1} d^{-1} for R2, by step-type disturbances in the inlet substrate concentration, keeping constant the percentage of COD composition. The feed flow rate (Q_f) was kept constant at 3.2 L d^{-1}. During these steps (I-III), the influent COD concentration was increased from 0.85 to 2.66 g L^{-1} containing around 5% of insoluble substrates principally composed of milk proteins. The sodium bicarbonate consumption for pH adjustment was increased from 0.66 to 2.43 g L^{-1} for both reactors. Finally, two steps in the feed flow rate from 3.2 to 4.3 L d^{-1} and from 4.3 to 6.0 L d^{-1}, keeping the same inlet concentration at 2.66 g COD L^{-1} for R1 and R2, were applied.

RESULTS AND DISCUSSION

The quantitative calibration of the model parameters is not an easy task with dynamical models for anaerobic digestion due the lack of some meassurements, the scarcity and uncertainty of others and the uncertainty related to the process

dynamics. Well known parameter data is used here and the less known parameter, the specific biofilm detachment rate, is estimated to obtain an appropriate agreement between the predicted and experimental values. The experimental measured variables were the bed height, total and soluble COD, VFA concentrations, pH, and gas concentration and flow rate.

Time variation of the experimental and predicted values of total and soluble COD for R1 and R2 are shown in Figures 2 (a, b) and 3 (a, b), respectively. Since the composition of the bioreactor feed is based on soluble substrates, the difference between total and soluble COD can be interpreted as an indirect measure of suspended biomass that leaves the reactor. For both reactors, more than 85% and 93% of total and soluble COD could be removed up to the maximum OLR applied, which indicates that the anaerobic fluidized bed system is very effective.

The differences between TCOD experimental and predicted values increase when the biofilm accumulation increases and when the lowest hydraulic retention times (HRTs, approximately 1.00 and 0.70 days for R1; 0.83 and 0.60 days for R2, measured from the expanded bed volumes) were used, i.e. when the disturbance steps (IV and V, Table 3) in the feed flow rate were applied. Here, parameters of the literature have been used and these, as well as some aspects of the non-active biomass hydrolysis model and the biofilm detachment model, should be revised.

Reactor 2 shows higher total and soluble COD values than R1 at the first organic loading step (Figs. 2 and 3). A high amount of suspended biomass for R2, which contains support particles with larger size than those of R1 (see Table 2), was experimentally observed. An increase in the particle diameter causes an increase in the biofilm detachment rate and a decrease in the specific surface for biofilm attachment.

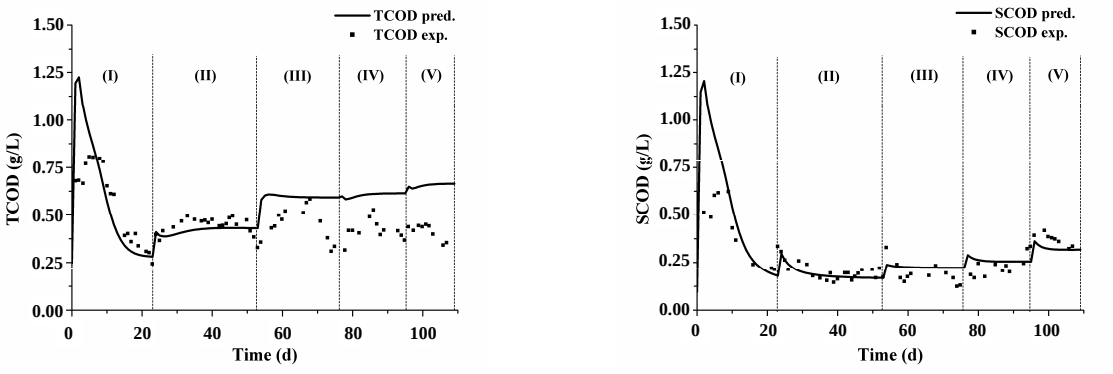

R1: (a) (b)

Figure 2: a) TCOD and b) SCOD experimental and predicted values for R1.

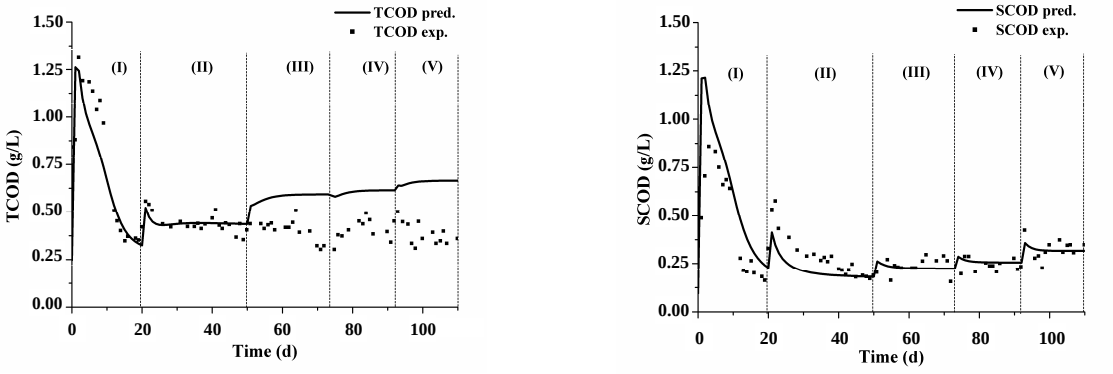

R2: (a) (b)

Figure 3: a) TCOD and b) SCOD experimental and predicted values for R2.

The major changes in the height of the bed were observed for R1 (Fig. 4). A decrease in the support particle diameter reduces the biofilm erosion and causes an increase in the biofilm accumulation (or biofilm thickness), making bioparticles be fluidized to a generally greater extension, accounting for a decrease in its specific gravity. Besides the biofilm accumulation, a sudden increase in the liquid velocity at the R1 inlet caused an increase in the height of the bed and a variation of the HRT from 1.12 to 1.30 days at the same feed flow rate of 3.2 L d^{-1} during the third organic loading step (Fig. 4). This hydrodynamic disturbance explains the OLR decrease in the start-up policy of R1 when compared to R2 (Table 3). An increase in the suspended biomass (and TCOD, Fig. 2a) was verified during this stage. This seems to indicate that the biofilm detachment rate is largely influenced by the liquid velocity at the reactor inlet (U_o). Figures 4 and 5 show experimental and predicted values of the bed height for R1 and R2, respectively. The dashed line in these figures represents the predicted values of the attached biomass (in grams).

Although a spherical geometry and homogeneous biofilm distribution on the inert support particles are assumed, in practice, the biofilm is normally inhomogeneously distributed on the real support particles. It depends on particle characteristics (shape, roughness, material porosity, size and weight) and on the hydrodynamic conditions, such as the fluid erosion on the bioparticle surface. In a previous work (Mussati et al., 2005b), it was observed by scanning electron microscopy (SEM) that microorganisms are attached to approximately 50% of the superficial area of sand particles, covering mainly the deep zones of the particles due to abrasion and erosion effects on the exposed zones.

Specific biofilm detachment rates $k_E = 3.73 \cdot 10^4$ $s^2\ kg^{-1}\ m^{-1}$ and $k_E = 0.75 \cdot 10^4$ $s^2\ kg^{-1}\ m^{-1}$ for R1 and R2, respectively, were estimated. An increase in k_E, over these values, predicts a decrease in the total biofilm concentration and time required to reach the biological steady state in each organic loading step.

The effluent soluble COD values were parallel to the effluent volatile fatty acids, as can be seen in Figures 6 and 7 (only acetate, propionate and butyrate have been represented) and compared with the results presented in Figures 2b and 3b for R1 and R2, respectively. This seems to indicate that the effluent SCOD is largely composed of the volatile fatty acids produced in the reactor.

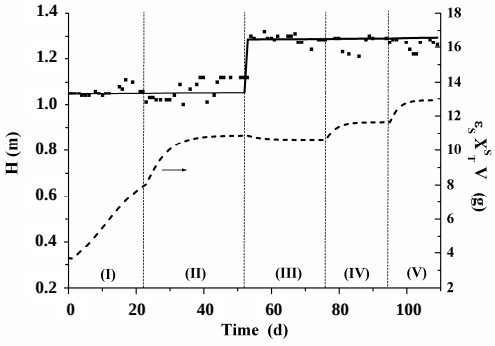

R1

Figure 4: Experimental and predicted values of the bed height and predicted values of the attached biomass for R1.

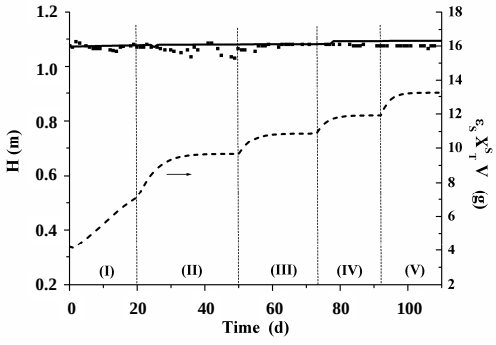

R2

Figure 5: Experimental and predicted values of the bed height and predicted values of the attached biomass for R2

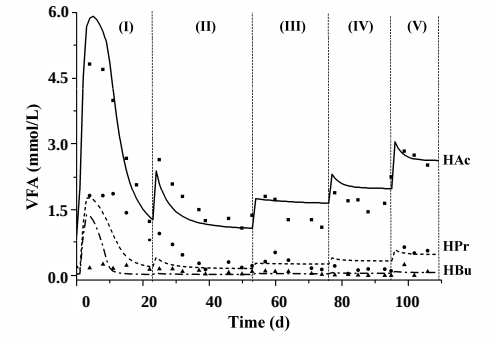

R1

Figure 6: VFA experimental and predicted values for R1.

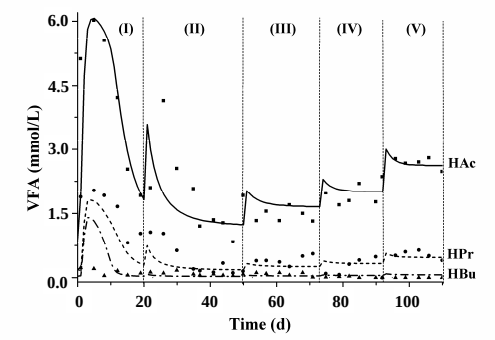

R2

Figure 7: VFA experimental and predicted values for R2.

Sodium bicarbonate addition was not superior to 2.43 g L^{-1} during step-type disturbances on the inlet concentration and feed flow rate, and total alkalinity was sufficient to maintain the system pH self-regulated at the typical operation range of methanogenic digesters (6.6-7.2) for both reactors (Figs. 8a and 9a).

The volumetric biogas production per day Q_G (and gas holdup) increased linearly with increased OLR for R1 (Fig. 8b) and R2 (Fig. 9b). Apparently, the activity of methanogenic microorganisms was not impaired up to operating OLR values for both reactors because of the adequate buffering capacities provided in the experimental systems. Chromatographic measurements of the composition of the gases accumulated in the gas collectors varied between 83 and 88% for CH_4, 15 and 10% for CO_2 and about 2% for other gaseous components.

The differences between experimental and predicted values of generated biogas decrease for the higher OLR values. Here, a constant liquid-gas mass transfer coefficient ($K_T = 100$ d^{-1}) has been assumed (Graef and Andrews, 1973). However, it is known that a variable mass transfer coefficient accounted much better for the gas production after a dynamic load than a constant one (Merkel and Krauth, 1999). These K_T correlations have been obtained as a function of several variables such as the substrate fed, liquid and reactor volumes, gas phase superficial velocity, and gas flow rate measured at the reactor outlet. The empiricism with which these correlations have been obtained led to the decision to use, as a first approach, a constant K_T for CO_2 in this work.

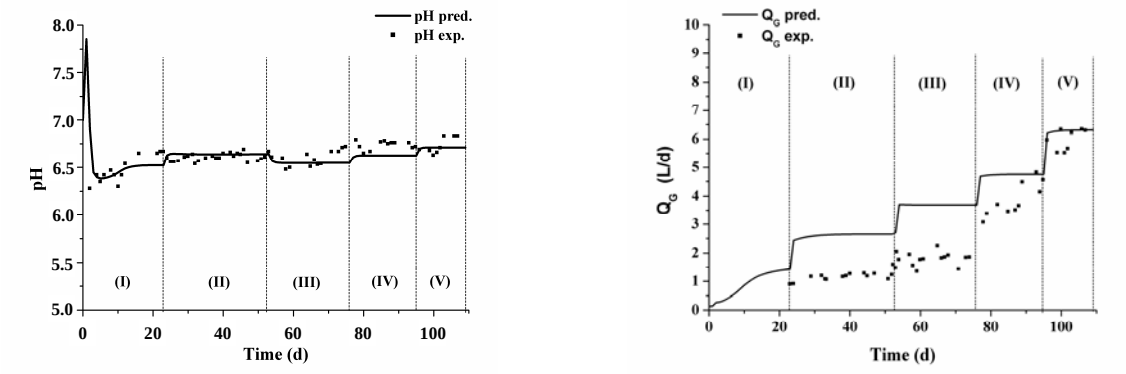

R1:(a) (b)

Figure 8: a) pH and b) gas flow rate for R1.

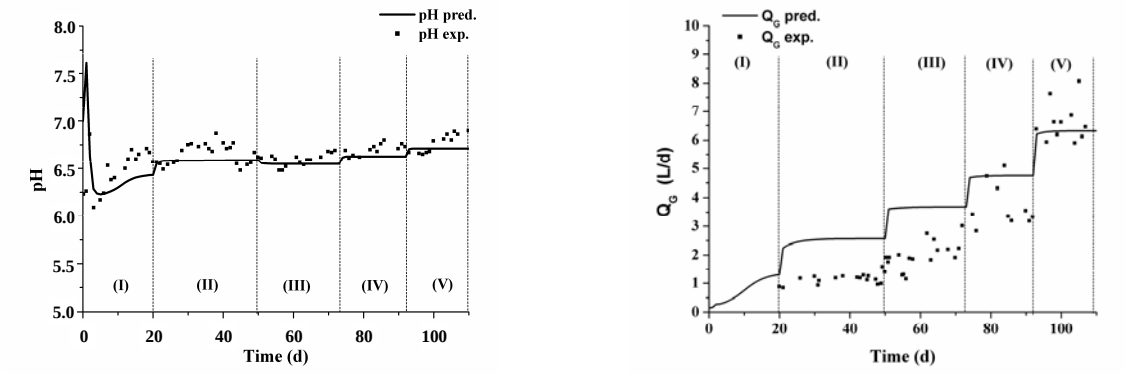

R2: (a) (b)

Figure 9: a) pH and b) gas flow rate for R2.

CONCLUSIONS

An appropriate agreement between the predicted and experimental values of soluble COD, VFA concentration, pH, biogas production rate and fluidized bed height was obtained by adjustment of the AFBR model proposed here, using well known parameter data for biological processes and the equilibrium in solution model and estimating the specific biofilm detachment rate k_E, for two mesophilic anaerobic lab-scale fluidized bed reactors (R1 and R2) with sand as support particles for biofilm attachment. Estimated values of k_E equal to $3.73 \cdot 10^4$ and $0.75 \cdot 10^4$ $s^2\ kg^{-1}\ m^{-1}$ for R1 and R2, respectively, were obtained. However, some aspects related to the biofilm detachment model and the hydrolysis of non-active biomass model should be revised to reproduce the total COD experimental values when the OLR increases.

High COD removal efficiency values (85% TCOD and 93% SCOD) were obtained during step-type disturbances in the influent concentration and feed flow rate, the biogas production rates showed the fastest responses to disturbances and the system pH was self-regulated at the typical operation range of methanogenic digesters for both reactors. The dynamic effects of the biofilm growth on the hydrodynamic and process components were studied. The simplified wake and bubble theory, used to calculate the fluidization characteristics, reproduced the main hydrodynamic events which took place in the reactors. The bioreactor model can be straightforwardly extended to different complex substrate degradation schemes.

ACKNOWLEDGMENTS

Financial support from Consejo Nacional de Investigaciones Científicas y Técnicas (CONICET), Agencia Nacional para la Promoción de la Ciencia y la Tecnología (ANPCyT) and Universidad Nacional del Litoral of Argentina is acknowledged.

NOMENCLATURE

Symbol

A	column cross sectional area	L^2
b	specific microorganism death rate	T^{-1}
d_{bp}	bioparticle diameter	L
d_p	particle diameter	L
g	gravity	LT^{-2}
H	bed height	L
k_E	specific biofilm detachment rate	$T^2\ M^{-1}\ L^{-1}$
K_H	Henry's coefficient	mol $atm^{-1}\ dm^{-3}$
K_{Hid}	specific hydrolysis rate	T^{-1}
K_T	total liquid-gas mass transfer coefficient	T^{-1}
n	bed expansion coefficient	
p	partial pressure	(atm)
Q	volumetric flow	$L^3\ T^{-1}$
R	bioprocess, mass transfer or transport process rate	$M\ L^{-3}\ T^{-1}$
Re_t	bioparticle terminal Reynolds number	
S	soluble substrate concentration	$M\ L^{-3}$
S_{ins}	insoluble substrate concentration	$M\ L^{-3}$
t	time	T
U_g	gas phase superficial velocity	$L\ T^{-1}$
U_l	liquid phase superficial velocity	$L\ T^{-1}$
U_t	particle terminal settling velocity	$L\ T^{-1}$
V	bed volume	L^3
W	support material load	M
X	biomass concentration	$M\ L^{-3}$
Y_{Si}	yield coefficient	$M\ M^{-1}$

Greeks Letters

δ	biofilm thickness	L
ε	k-phase holdup, porosity ($\varepsilon = \varepsilon_L + \varepsilon_G$)	
$\lambda_{S_i}^j$	+1, -1, 0, stoichiometric coefficient	
μ	specific microorganism growth rate	T^{-1}
μ_L	liquid viscosity	$M\ L^{-1}\ T^{-1}$
ν_{st}	gas standard volume	$L^3\ M^{-1}$
ρ	density	$M\ L^{-3}$
ω	energy dissipation parameter	$M\ T\ L^{-1}$
φ	concentration	$M\ L^{-3}$

Subscripts and Superscripts

a	active (biomass)
Aa	amino acids
Ac	acetate
Bu	butyrate
CH_4	methane

CO_2	carbon dioxide
f	bioreactor feed
G	referred to gas phase
Gl	glucose
i	species index
IC	inorganic carbon
in	referred to reactor inlet
IN	inorganic nitrogen
j	bioprocess, mass transfer and transport process index
k	phase index
L	referred to liquid phase
na	non-active (biomass)
o	static bed condition
out	referred to reactor outlet
Pr	propionate
S	referred to solid phase
T	total
Va	valerate

REFERENCES

Abdul-Aziz, M. A. and Asolekar, S. R., Modeling of Biological Particle Mixing in a Fluidized-Bed Biofilm Reactor, Water Environ. Res., 72, 105-115 (2000).

Angelidaki, I., Ellegaard, L. and Ahring, B. K., A Mathematical Model for Dynamic Simulation of Anaerobic Digestion of Complex Substrates: Focusing on Ammonia Inhibition, Biotechnol. Bioeng., 42, 159-166 (1993).

Angelidaki, I., Ellegaard, L. and Ahring, B.K., A Comprehensive Model of Anaerobic Bio-conversion of Complex Substrates to Biogas, Biotechnol. Bioeng., 63, 363-372 (1999).

Bhatia, V. K. and Epstein, N., Three Phase Fluidization: a Generalized Wake Model. In Proceedings of the International Syrup. Fluid. Appl., Cepadues-Editions, Toulouse, 380-392 (1974).

Bonnet, B., Dochain, D. and Steyer, J. P., Dynamical Modeling of an Anaerobic Digestion Fluidized Bed Reactor, Water Sci. Technol., 36(5), 285-292 (1997).

Chern, S. H., Fan, L. S. and Muroyama, K., Hydrodynamics of Concurrent Gas-liquid-solid Semifluidization with a Liquid as the Continuous Phase, AICHE J., 30, 288-294 (1984).

Diez Blanco, V., García Encina, P. A., Fdz-Polanco, F., Effects of Biofilm Growth, Gas and Liquid Velocities on the Expansion of Anaerobic Fluidized Bed Reactor (AFBR), Water Res. (G.B.), 29(7), 1649-1654 (1995).

Efremov, G. I. and Vakhrushev, I. A., A Study of the Hydrodynamics of Three-phase Fluidized Beds, Int. Chem. Eng., 10, 37-4l (1970).

Foscolo, P. U., Gilibaro, L. G. and Waldarm, S. P., A Unified Model for Particulate Expansion of Fluidized Beds and Flow in Fixed Porous Media, Chem. Eng. Sci., 38(8), 1251-1260 (1983).

Graef, S.P. and Andrews, J., Mathematical Modeling and Control of Anaerobic Digestion. AICHE Symposium Series, 70 (136), 101-131 (1973).

Hermanowicz, S. W. and Ganzarczyk, J. J., Some Fluidization Characteristics of Biological Beds, Biotechnol. Bioeng., 25, 1321-1330 (1983).

Huang, J. and Wu, C., Specific Energy Dissipation Rate for Fluidized Bed Bioreactors, Biotechnol. Bioeng., 50, 643-654 (1996).

Huang, J., Yan, J. and Wu, C., Comparative Bioparticle and Hydrodynamic Characteristics of Conventional and Tapered Anaerobic Fluidized-bed Bioreactors, J. Chem. Technol. Biot., 75, 269-278 (2000).

McCabe, W. L., Smith, J. C. and Harriott, P., Unit Operations of Chemical Engineering, McGraw-Hill Book Co, New York (1993).

Merkel, W. and Krauth, K., Mass Transfer of Carbon Dioxide in Anaerobic Reactors under Dynamic Substrate Loading Conditions. Wat. Res. 33 (9), 2011-2020 (1999).

Miyahara, T. and Fan, L. S., Properties of a Large Bubble in a Bubble Swarm in a Three-phase Fluidized Bed, J. Chem. Eng. Jpn., 25, 378-382 (1992).

Mulcahy, L. T. and Shieh, W. K., Fluidization and Reactor Biomass Characteristics of the Denitrification Fluidized Bed Biofilm Reactor, Water Res. (G.B.) 21, 451-458 (1987).

Muroyama, K. and Fan, L. S., Fundamentals of Gas-liquid-solid Fluidization, AICHE J. 31, 1-34 (1985).

Mussati, M., Aguirre, P., Fuentes, M. and Scenna, N., Aspects on Methanogenic Biofilm Reactor Modeling, Lat. Am. Appl. Res., 36, 173-180 (2006).

Mussati, M., Fuentes, M., Aguirre, P. and Scenna, N., A Steady-state Module for Modeling Anaerobic Biofilm Reactors, Lat. Am. Appl. Res., 35, 255-263 (2005a).

Mussati, M., Thompson, C., Fuentes, M., Aguirre, P. and Scenna, N., Characteristics of a Methanogenic Biofilm on Sand Particles in a Fluidized Bed Reactor, Lat. Am. App. Res., 35, 265-272 (2005b).

Ngian, K. F. and Marti, W. B., Bed Expansion Characteristics of Liquid Fluidized Particles with

Attached Microbial Growth, Biotechnol. Bioeng., 22, 1843-1856 (1980).

Perry, R. H. and Chilton, C. H., Chemical Engineers' handbook, McGraw-Hill, New York (1973).

Richardson, J. F. and Zaki, W. N., Sedimentation and Fluidization, Part 1, Trans. Inst. Chem. Eng., 32, 35-53 (1954).

Setiadi, T., Predicting the Bed Expansion of an Anaerobic Fluidized Bed Bioreactor. Water Sci. Technol., 31, 181-191 (1995).

Thomas, C. R. and Yates, J. G., Expansion Index for Biological Fluidized Beds, J. Inst. Chem. Eng., 63, 67-70 (1985).

Yu, H. and Rittmann, B. E., Predicting Bed Expansion and Phase Holdups for Three-Phase Fluidized-Bed Reactors with and without Biofilm, Water Res., 31, 2604-2616 (1997).